



## An empirical approach for the retrieval of integral ocean wave parameters from synthetic aperture radar data

J. Schulz-Stellenfleth,<sup>1</sup> T. König,<sup>1</sup> and S. Lehner<sup>1</sup>

Received 13 October 2006; revised 18 October 2006; accepted 1 November 2006; published 29 March 2007.

[1] In this study a new empirical approach to retrieve integral ocean wave parameters from synthetic aperture radar (SAR) data is presented. The idea behind this computationally efficient technique is to estimate integral ocean wave parameters without the intermediate step of retrieving the two-dimensional ocean wave spectrum. The method has the radiometrically calibrated SAR image as the only source of information and is based on a quadratic model function with 22 input parameters. These parameters include the radar cross section, the image variance, and 20 parameters computed from the SAR image variance spectrum using a set of orthonormal functions. The coefficients of the quadratic function were fitted for the estimation of  $H_s$ , the mean periods  $T_{m01}$ ,  $T_{m02}$ ,  $T_{-10}$ , the wave power, and the wave heights associated with different spectral bands. The fit procedure is based on a stepwise regression method. A data set of 12,000 globally distributed ERS-2 wave mode image spectra and colocated WAM ocean wave spectra was available for the study. Two separate subsets of 6000 collocation pairs each were used to fit the model and to carry out comparisons of the retrieved wave parameters with numerical model results. Additional comparisons were performed using NDBC buoy measurements. Scatterplots and global maps with the derived parameters are presented. It is shown that the rms of the SAR derived  $H_s$  with respect to the WAM  $H_s$  is about 0.5 m. For the mean period  $T_{m-10}$  an rms of 0.72 s with a high-frequency cutoff period of about 6 s is achieved.

**Citation:** Schulz-Stellenfleth, J., T. König, and S. Lehner (2007), An empirical approach for the retrieval of integral ocean wave parameters from synthetic aperture radar data, *J. Geophys. Res.*, 112, C03019, doi:10.1029/2006JC003970.

### 1. Introduction

[2] It is well known that synthetic aperture radar (SAR) data contain valuable information on ocean surface waves [Alpers *et al.*, 1981; Hasselmann and Hasselmann, 1991]. Operating in Wave Mode, the European satellites ERS-1, ERS-2, and ENVISAT have been acquiring SAR data on a global and continuous basis for about 15 years by now. These acquisitions will be continued by the new Sentinel-1 mission, which will have a Wave Mode as well [Attema, 2005].

[3] There is still a lot of debate about efficient techniques to retrieve wave parameters from SAR data. If the objective is to estimate the two-dimensional (2-D) ocean wave spectrum, there are basically two approaches. In the first approach the measurement is restricted to the long wave regime accepting the fact that some information on shorter waves is lost [Johnsen *et al.*, 2002]. The second approach estimates the complete 2-D wave spectrum using some additional a priori information, e.g., taken from numerical ocean wave models [Hasselmann *et al.*, 1996; Schulz-Stellenfleth *et al.*, 2005a] or from other sensors

[Mastenbroek and de Valk, 2000]. The approaches described by Hasselmann *et al.* [1996] and Schulz-Stellenfleth *et al.* [2005a] are of particular relevance for the assimilation of numerical ocean wave models and the scheme developed at the Max-Planck-Institute for Meteorology [Hasselmann *et al.*, 1996] is in fact currently run operationally at the European Centre for Medium-Range Weather Forecasts (ECWMF) [Abdalla *et al.*, 2006].

[4] Although the existing methods already provide useful wave information, it seems there is still potential to exploit SAR data more efficiently. In this paper a new empirical approach is presented, which has the objective to estimate integral wave parameters like the significant wave height  $H_s$  or the mean wave period from SAR data without explicit retrieval of the 2-D ocean wave spectrum. The main requirements for the development of the method were as follows: (1) The estimation of the wave parameters should be solely based on the SAR data. (2) The method should provide estimates of standard integral wave parameters like  $H_s$  used in practical applications. (3) The method should be computationally efficient. The first point is of particular importance for users of SAR data without easy access to numerical model data. It is also important to note that the new ENVISAT satellite, unlike the earlier ERS-1 and ERS-2 platforms, does not carry a scatterometer, i.e., the approach presented by Mastenbroek and de Valk [2000] to use a combination of scatterometer and SAR measurements to

<sup>1</sup>Remote Sensing Technology Institute, German Aerospace Center (DLR), Oberpfaffenhofen, Germany.

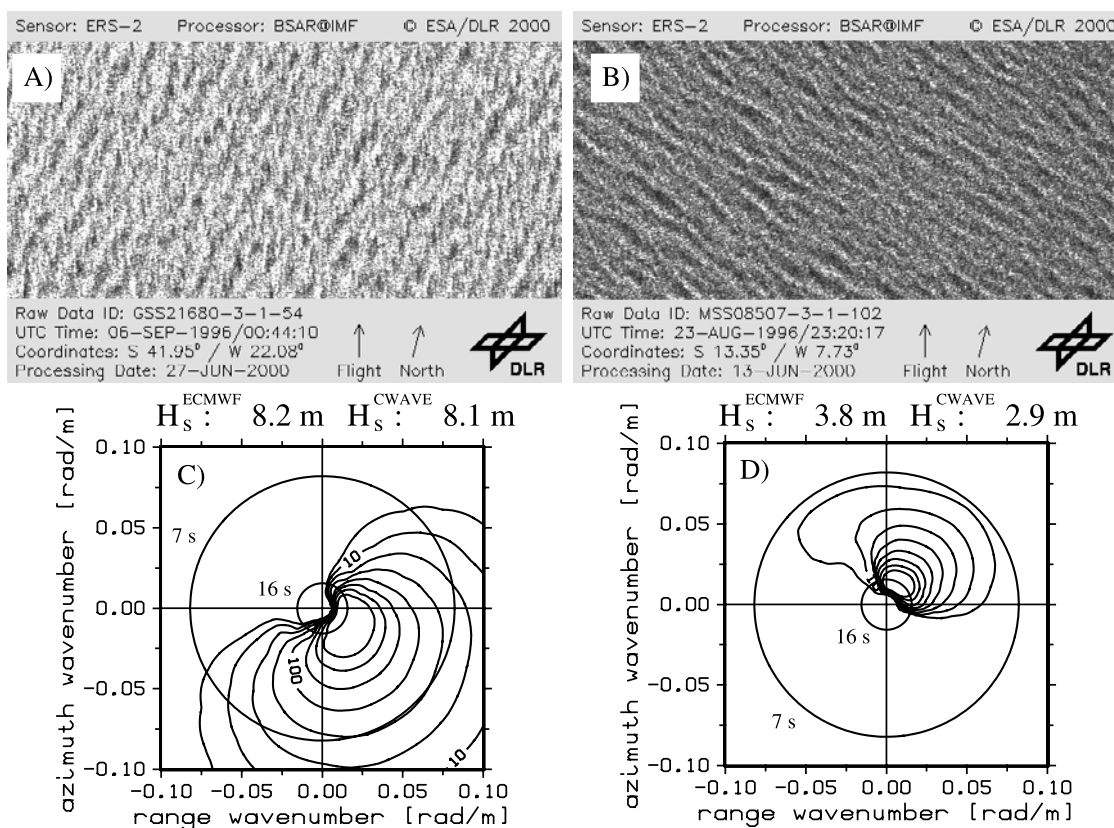


**Figure 1.** (a and b) Two ERS-2 Wave Mode imagerettes and (c and d) corresponding ECMWF wave model spectra taken in the South Atlantic ocean with Figures 1a and 1c representing a strong wind sea and Figures 1b and 1d representing a swell system.

estimate wave parameters is not possible with ENVISAT and will neither be applicable with the future Sentinel-1 mission.

[5] The idea of the present approach is to fit a quadratic model which relates a number of key parameters of SAR scenes taken over the ocean, like the normalized radar cross section (NRCS) or the image variance to different integral ocean wave parameters. The main feature of the technique is that no explicit estimation of the two-dimensional ocean wave spectrum is carried out as an intermediate step as done in all other methods that we are aware of. We will refer to the general empirical approach as the CWAVE method in the following. The name was chosen to indicate a similarity of our approach with the empirical CMOD models used for scatterometer wind measurements [Stoffelen and Anderson, 1997]. The specific formulation of the empirical model and the tuning parameters presented in this paper are referred to as CWAVE2.0 to separate it from the CWAVE1.0 approach described in [Schulz-Stellenfleth et al., 2005b]. We expect that with the availability of new tuning data sets, updates of the scheme will be carried out in the future.

[6] The paper is structured as follows: In section 2 the data sets used for the study are introduced. Section 3 is about the general approach of the CWAVE2.0 method. In section 4 a simple version of the method is presented using two SAR parameters for the estimation of the significant wave height to illustrate the basic features of the technique. This simple approach is then extended to a set of 22 SAR parameters in section 5 using additional spectral informa-

tion. In section 6 CWAVE2.0 derived wave heights are compared to in situ data provided by NASA's National Data Buoy Center (NDBC).

## 2. Data Sets

[7] To fit and test the CWAVE2.0 model, a colocated data set of 12,000 ERS-2 wave mode images and corresponding 2-D ocean wave spectra from the ocean wave model WAM run at ECMWF is used. Both data sets are described in the following.

### 2.1. ERS-2 Wave Mode Data

[8] Operating in Wave Mode, the ERS-2 satellite acquires SAR images (imagerettes) of 10 by 5 km size every 200 km along the satellite track. The C-band radar operates at 23.5° incidence angle with vertical polarization in transmit and receive and provides a spatial resolution of about 10 m in azimuth and 20 m in ground range. The required SAR Wave Mode single look complex (SLC) imagerettes, which are not available as standard products were processed at DLR from raw data provided by the European Space Agency (ESA). More details on the reprocessed data set can be found in the work of Lehner et al. [2000].

[9] For tuning and testing of the algorithm, a data set of globally distributed images acquired between 23 August and 8 September 1996 was used. Two examples of SAR imagerettes taken in the South Atlantic are shown in Figures 1a and 1b. The first case (Figure 1a) shows a strong wind sea of

more than 8 m wave height, whereas the second example (Figure 1b) represents a swell-dominated situation.

[10] For the estimation of the different SAR parameters, only imagerettes were considered, which were acquired between 60S and 60N latitude to avoid contamination by sea ice. The homogeneity test described by *Schulz-Stellenfleth and Lehner* [2004] was applied to the remaining data. This test is able to detect images affected by atmospheric features like rain or biogenic surface films, which should not be used in the fitting process or the subsequent application of the fitted CWAVE2.0 model. About 17% of the imagerettes failed to pass this test. After excluding those cases for which no colocated wave model spectrum was available, the remaining number of images was 12,000. A global map with the number of imagerettes per 3 by 3 degree box is shown in Figure 9a.

[11] The data set was split into the four time intervals 23.8–26.8, 26.8–30.8, 30.8–4.9, and 4.9–8.9.1996. The respective subsets are disjunct and contain 3000 images each. The first and third subset were used for testing and the second and fourth subset were used for tuning of the algorithm.

[12] As the normalized radar cross section is an important input parameter for the CWAVE2.0 model, a radiometric calibration was carried out using the calibration constant estimated by *Horstmann et al.* [2003]. Denoting the complex image with  $c$  and the intensity image with  $I = |c|^2$ , a first estimate of the NRCS is given by

$$\sigma_0^pl = 10 \log_{10} (\langle I \rangle) - 44.96 \text{ dB}, \quad (1)$$

where  $\langle I \rangle$  is the mean imagerette intensity. This estimate is affected by a saturation of the ADC converter on board the satellite [*Laur et al.*, 1996], which becomes significant for high wind speeds. An estimate of the power loss corrected NRCS

$$\sigma_0 = \sigma_0^pl + \Delta\sigma_0 \quad (2)$$

was calculated as described by *Kerbaol et al.* [1998] using the I/Q channel standard deviation calculated from the SAR raw data as additional information. For the examples shown in Figure 1 this procedure results in a power loss corrected NRCS of  $-1.68$  dB (Figure 1a) and  $-6.13$  dB (Figure 1b), respectively.

## 2.2. Numerical Wave Model Data

[13] The 2-D ocean wave spectra used in the study are standard output from the operational WAM model runs performed at ECMWF in 1996 at the four synoptical hours 0000, 0600, 1200, and 1800 UTC. The temporal gap between WAM and SAR measurement is thus less than 3 hours. The model was driven by 6-hourly analyzed  $U_{10}$  wind fields computed with the atmospheric general circulation model (AGCM). The operational WAM model was run with a  $1.5^\circ \times 1.5^\circ$  latitude-longitude grid. The collocation distance to the ERS-2 imagerettes is thus less than  $0.75^\circ$ . The 2-D wave spectra are given on a polar grid with  $30^\circ$  directional resolution and 25 frequencies ranging from  $f_{min} = 0.04177$  Hz to  $f_{max} = 0.41$  Hz. Details on the performance of the ECMWF model in 1996 can be found in the work of *Janssen et al.* [1997] and *Bidlot et al.* [2002].

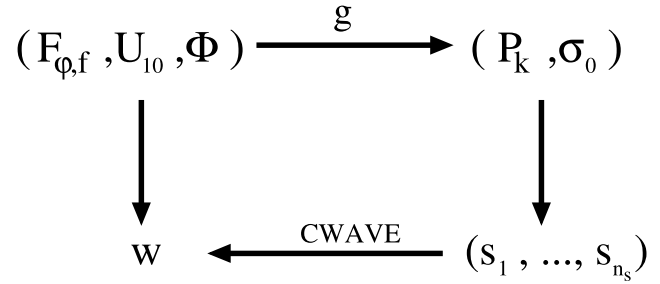


**Figure 2.** Diagram illustrating the relationship between the ocean wave spectrum  $F_{\phi,f}$ , the integral wave parameter  $w$ , the wind speed  $U_{10}$ , the wind direction  $\Phi$ , the SAR image spectrum  $P_k$ , the radar cross section  $\sigma_0$ , and the SAR parameter vector  $(s_1, \dots, s_{n_s})$  (see text for details).

[14] The colocated 2-D wave spectra for the examples in Figures 1a and 1b are shown in Figures 1c and 1d. The maximum ECMWF wind speeds colocated with the ERS-2 wave mode data set is shown in Figure 9b. One can see several strong storm areas in particular on the southern hemisphere. In addition there are some higher wind speeds observed in the North Atlantic due to Hurricane Fran.

[15] It is important to note that the performance of the ECMWF model has steadily improved since 1996. Details on the model development can be found in the work of *Janssen* [2004] and *Janssen et al.* [2005].

## 3. General Approach

[16] The general approach of the CWAVE method is illustrated in the diagram shown in Figure 2. Physical models were proposed in literature [*Hasselmann and Hasselmann*, 1991], which describe the mapping process  $g: (F_{\phi,f}, U_{10}, \Phi) \rightarrow (P_k, \sigma_0)$ , where  $F_{\phi,f}$  is the directional frequency ocean wave spectrum,  $U_{10}$  is the wind speed,  $\Phi$  is the wind direction,  $P_k$  is the variance spectrum of the normalized SAR image, and  $\sigma_0$  is the mean radar cross section. It is well known that the function  $g$  is not one-to-one and considerably nonlinear. The derivation of 2-D ocean wave spectra from SAR data is therefore not a trivial task [*Hasselmann et al.*, 1996; *Schulz-Stellenfleth et al.*, 2005a] and usually requires some a priori information.

[17] The approach in this study is therefore to estimate an integral ocean wave parameter  $w$  from a set of SAR parameters  $s_1, \dots, s_{n_s}$  directly. The idea is that although the SAR parameters are generally not sufficient to estimate the complete wave spectrum, they may well be sufficient to provide useful information on certain parameters derived from this spectrum. We consider wave parameters  $w$ , which are computed from the directional frequency ocean wave spectrum  $F_{\phi,f}$  according to

$$w = \left( \frac{1}{m_0^\nu} \int_0^{2\pi} \int_{f_{min}}^{f_{max}} F_{\phi,f} T_f^w d\phi df \right)^\nu, \quad (3)$$

where  $T_f$  is a weighting function and the zero-order moment  $m_0$  is defined as

$$m_0 = \int_0^{2\pi} \int_{f_{min}}^{f_{max}} F_{\phi,f} d\phi df. \quad (4)$$

For the wave parameters considered here,  $\nu$ ,  $\mu$  are rational numbers with  $\nu \in \{-1, 1/2, 1\}$  and  $\mu \in \{0, 1\}$ .

[18] The derivation of the CWAVE2.0 model for ocean wave parameter estimation is based on a least squares minimization procedure. The model function has a set of  $n_S$  SAR parameters

$$\mathbf{s} = (s_1, \dots, s_{n_S}) \quad (5)$$

as input. In this study the NRCS, the image variance and a number of spectral parameters introduced in section 5 are used for this purpose. To take into account nonlinearities as well as a possible coupling between these parameters, the following quadratic formulation is used:

$$w = a_0 + \sum_{1 \leq i \leq n_S} a_i s_i + \sum_{1 \leq i < j \leq n_S} a_{ij} s_i s_j \quad (6)$$

This formulation can be regarded as the Taylor expansion up to second order of the function  $h: (s_1, \dots, s_{n_S}) \rightarrow w$ . Even if it is not clear in all detail yet what the physical basis for this function is, the empirical approach still provides analytical information on the structure of the mapping process.

[19] The tuning parameters are collected into a vector

$$\mathbf{A} := (A_0, \dots, A_{n_f-1}) := (a_0, \dots, a_{n_S}, a_{11}, \dots, a_{n_S n_S}) \quad (7)$$

of dimension

$$n_f = 0.5(n_S^2 + 3n_S + 2). \quad (8)$$

The SAR parameters and their respective products are summarized in a corresponding vector

$$\mathbf{S} = (S_0, \dots, S_{n_f-1}) = (1, s_1, \dots, s_{n_S}, s_1 s_1, \dots, s_{n_S} s_{n_S}) \quad (9)$$

of equal length. The tuning parameters are then fitted based on the minimization of a cost function

$$J_{\text{cost}}(\mathbf{A}) = \sum_{j=1}^N \left( \mathbf{w}^{(j)} - \sum_{i=0}^{n_f-1} \mathbf{A}_i \mathbf{S}_i^{(j)} \right)^2, \quad (10)$$

where  $(w^{(1)}, \mathbf{S}^{(1)}), \dots, (w^{(N)}, \mathbf{S}^{(N)})$  represent the available collocation pairs of SAR acquisitions and ocean wave model data described in section 2. The cost function defines a standard quadratic minimization problem which was solved using a singular value decomposition technique as described in Appendix A.

[20] Once the model parameters  $\mathbf{A}$  are fitted, the wave parameter  $w$  is estimated from a given SAR parameter vector  $\mathbf{S}$  according to

$$w \approx \sum_{i=0}^{n_f-1} A_i S_i. \quad (11)$$

It is important to say that the cost function formulation equation (10) is based on the simple assumption that the deviation between the quadratic model and the numerical wave model is Gaussian distributed with the same variance for all collocation pairs and all sea states. By introducing weighting factors in the cost function, it would be possible

to take into account the variability of collocations distances in space and time as well as a possible sea state dependence. However, to keep the presentation simple we will work with the formulation equation (10) in this study.

[21] Another point to be emphasized is the fact that the tuned model depends on the distribution of the wave model data used in the tuning exercise. This can be illustrated with a strongly simplifying example. Let us assume that the wave spectrum has two bins  $F = (F_1, F_2)$  only. Furthermore, we consider a single SAR parameter  $s$ , which is connected to the wave spectrum by

$$s = \alpha F_1 + \beta F_2 \quad (12)$$

in a linear and deterministic way with two SAR imaging parameters  $\alpha$ ,  $\beta$ . If we try to estimate a wave parameter  $w$  defined as

$$w = F_1 + F_2 \quad (13)$$

from  $s$  using a linear model

$$w = a_1 s + a_0 \quad (14)$$

it is straightforward to show that a least squares approach (with an infinite large tuning data set) results in

$$a_1 = \frac{\alpha \rho_{F_1 F_1} + \beta \rho_{F_2 F_2} + (\alpha + \beta) \rho_{F_1 F_2}}{\alpha^2 \rho_{F_1 F_1} + 2\alpha\beta \rho_{F_1 F_2} + \beta^2 \rho_{F_2 F_2}} \quad (15)$$

$$a_0 = \langle F_1 \rangle (1 - \alpha a_1) + \langle F_2 \rangle (1 - \beta a_1), \quad (16)$$

where the angle brackets denote the mean and  $\rho_{F_1 F_1}$ ,  $\rho_{F_2 F_2}$ ,  $\rho_{F_1 F_2}$  are the variances and covariance of the wave spectrum  $F$  respectively. As one can see, the model depends on the statistical properties of  $F$  in general. Only for special cases, e.g.,  $\alpha = \beta$  (leading to  $a_1 = \alpha^{-1}$  and  $a_0 = 0$ ), the model is solely determined by the SAR imaging parameters. The case  $\alpha = \beta$  represents the ideal situation where the SAR parameter  $s$  contains the full information about the wave parameter  $w$ . With the additional nonlinear mechanisms observed in practice this is a very hard to achieve scenario, however. As a consequence, one has to accept the fact that the tuning data set is one of the key factors for the empirical approach. The choice of data is certainly a critical issue that needs some further consideration, e.g., by using triple collocations with additional buoy data. Owing to the lack of suitable data sets, we will not discuss this issue further in this study.

### 3.1. Stepwise Regression

[22] To keep the CWAVE2.0 model compact and to avoid that the expansion equation (6) contains many terms which do not lead to a significant improvement of the model a stepwise regression method as, e.g., described by *von Storch and Zwiers* [1999] is used. In the forward selection approach a linear model is fitted for a subset of SAR parameters  $\mathbf{S}^{(k)} = (S_{z(1)}, \dots, S_{z(k)})$ , which is extended by one element in each step. The quality of the iterated models is assessed using the sum of squares due to regression (SSR)

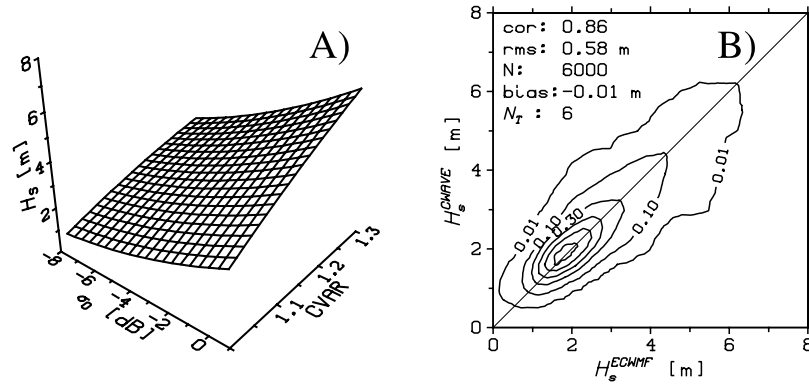


**Figure 3.** (a) Significant wave height  $H_s$  as a function of normalized radar cross section  $\sigma_0$  and image variance  $cvar$ . The functional dependence is the result of a fit procedure using 6000 ERS-2 wave mode images and colocated ECMWF wave model data. (b) Scatterplot of significant wave height derived from equation (11) versus ECMWF wave heights derived from a separate data set of 6000 collocation pairs.

and the sum of squared errors (SSE) calculated in each iteration step as

$$SSR^{(k)} = \sum_{j=1}^N \left( \bar{w} - \sum_{i=0}^k A_{z(i)} S_{z(i)}^{(j)} \right)^2 \quad (17)$$

$$SSE^{(k)} = \sum_{j=1}^N \left( w^{(j)} - \sum_{i=0}^k A_{z(i)} S_{z(i)}^{(j)} \right)^2 \quad (18)$$

where  $\bar{w}$  is the mean of the wave parameter  $w$ . The  $SSR$  parameter is a measure for the ability of the linear model to explain the variability in the data set, i.e.,  $SSR$  should be high. Consequently, the new parameter  $S_{z(k+1)}$  added in the next iteration step is chosen such that  $SSR^{(k+1)} - SSR^{(k)}$  is maximized. To check whether this increase is statistically significant, the variable

$$F^{(k+1)} = \frac{SSR^{(k+1)} - SSR^{(k)}}{SSE^{(k+1)}(N - k)^{-1}} \quad (19)$$

which is  $F(1, N-k)$  distributed [von Storch and Zwiers, 1999] is used. The iteration is terminated at some step  $k = N_T$  if the test variable  $F^{(k+1)}$  is below the 99% confidence limit as given by the F-statistics. In this paper we describe the above fitting procedure for different wave parameters  $w$  and different SAR parameter vectors  $\mathbf{S}$ .

#### 4. A Two-Parameter Model for $H_s$

[23] In this section a simple two SAR parameter model is fitted for the estimation of the significant wave height  $H_s$  to illustrate the general approach. For this purpose the variance of the normalized SAR image  $cvar$  [Kerbaol et al., 1998] and the power loss corrected NRCS  $\sigma_0$  are taken as input for the model. The parameter  $cvar$  is defined as the variance of the normalized intensity image

$$\bar{I} = \frac{I - \langle I \rangle}{\langle I \rangle} \quad (20)$$

i.e.,  $cvar$  is scaling invariant with respect to the NRCS. In this case the vector  $\mathbf{S}$  defined in equation (9) has the form

$$\mathbf{S} = (1, \sigma_0, cvar, \sigma_0^2, \sigma_0 cvar, cvar^2). \quad (21)$$

The idea behind this particular choice of SAR parameters is that both  $\sigma_0$  and  $cvar$  contain information on the ocean wave energy. The parameter  $cvar$  is the integral of the SAR image variance spectrum, which has a complicated dependence on the 2-D ocean wave spectrum as analyzed in many studies [Hasselmann and Hasselmann, 1991; Alpers et al., 1981]. The SAR spectrum mainly contains information on the longer waves. The normalized radar cross section on the other hand is directly related to the local wind field [Stoffelen and Anderson, 1997; Lehner et al., 1998], which in turn has an impact on the shorter wind sea waves. Furthermore, there is some indication that the local wind speed also has some influence on the variance of the normalized intensity image [Mastenbroek and de Valk, 2000]. The coupling term in the second order model to some extent allows to take such mechanisms into account.

[24] The model was tuned with the fit data set described in section 2 comprising 6000 collocation pairs. In this case the model was fitted for the estimation of the significant wave height, i.e.,  $w = H_s$  in equation (6). Here,  $H_s$  is computed from the WAM spectrum according to

$$H_s = 4 \left( \int_0^{2\pi} \int_{f_{\min}}^{f_{\max}} F_{\phi f} df d\phi \right)^{1/2} \quad (22)$$

with the directional frequency spectrum  $F_{\phi f}$  and  $f_{\min}$  and  $f_{\max}$  defined in section 2, i.e., the wave height refers to all wave components contained in the model spectrum.

[25] The fit procedure resulted in the following components of the vector  $\mathbf{A}$  defined in equation (7)

$$\mathbf{A} = \left( -18.26 \text{ m}, -0.259 \frac{\text{m}}{\text{dB}}, 28.21 \text{ m}, 0.0189 \frac{\text{m}}{\text{dB}^2}, 0.672 \frac{\text{m}}{\text{dB}}, -7.37 \text{ m} \right). \quad (23)$$

In this case the stepwise regression described in section 3.1 indicates that all six terms in the quadratic model are statistically significant.

[26] The resulting functional dependence of the wave height  $H_s$  on the two SAR parameters is shown in Figure 3a. One can see that the wave height is increasing with growing radar cross

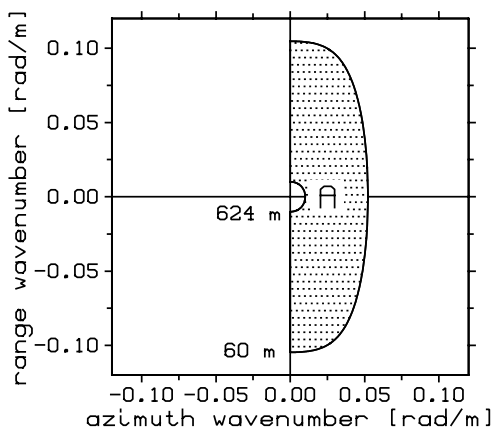


**Figure 4.** Integration area  $A$  in the SAR image wave number domain used by the empirical CWAVE2.0 algorithm to extract spectral ocean wave information by means of the orthogonal functions defined in equation (B13).

section and image variance. Small nonlinear effects and coupling of the parameters are visible as well.

[27] A comparison of ECMWF and CWAVE derived significant wave heights using the test data set of 6000 collocation pairs described in section 2 is shown in Figure 3b. As one can see, even this simple approach already gives a reasonable correlation of 0.86 and an rms of 0.58 m with negligible bias. For the two examples in Figure 1,  $cvar$  is estimated as 1.46 (Figure 1a) and 1.31 (Figure 1b), respectively. With the  $\sigma_0$  values given in section 2 the two parameter model gives significant wave heights of 6.1 m (A) and 2.9 m (B). In both cases, the two-parameter CWAVE wave heights are underestimated with respect to the ECMWF analysis, in particular for case A.

[28] A similar approach was also carried out using the azimuthal cutoff wavelength estimated from the SAR image spectrum, e.g., described by Kerbaol [1997] as an additional parameter. The idea is that according to the standard theory the cutoff wavelength is supposed to be strongly related to the energy in the high-frequency part of the wave spectrum. However, it turned out that this extension does not improve the results. This could be due to problems in the estimation of the cutoff wavelength and the fact that a lot of information this parameter contains about shorter waves is already provided by  $\sigma_0$ . In the next section we present an approach where more detailed information about the shape of the 2-D SAR image spectrum is used.

## 5. Extended Model With Additional Spectral Information

[29] In this section we extend the two-parameter approach described in the previous section using more detailed information taken from the 2-D SAR image variance spectrum. This model is then applied for the estimation of  $H_s$ , the wave heights contained in different spectral bands, different mean wave periods, and the wave power  $J$ .

[30] The extraction of the spectral parameters is based on a set of orthonormal functions, which are defined in the spectral regime  $A$  indicated in Figure 4. The area  $A$  was

chosen such that it covers the regime where most of the spectral energy of the ERS-2 wave mode data can be found [Lehner et al., 2000]. In particular the elliptical shape takes into account the velocity bunching effect, which leads to a low pass filtering and bunching of the spectrum in the azimuth direction. The orthonormal functions are constructed as tensor products of special polynomials and harmonics defined in the direction-wave number space. The respective dimensions are denoted by  $n_\varphi$  and  $n_k$ . The exact definition of the orthonormal functions  $\bar{h}_i$ ,  $i = 1, \dots, n_\varphi n_k$  is given in Appendix B. By definition, the functions satisfy

$$\int_A \bar{h}_i(k_x, k_y) \bar{h}_{i'}(k_x, k_y) dk_x dk_y = \delta_{i-i'} \quad 1 \leq i, i' \leq n_\varphi n_k. \quad (24)$$

The functions  $\bar{h}_1, \dots, \bar{h}_9$  are visualized in Figure 5 for  $n_\varphi = 3$  and  $n_k = 3$ . The grey values have a linear scaling between  $-80$  m (black) and  $+80$  m (white).

[31] The SAR parameters to be used for the CWAVE2.0 model are then computed from the SAR image spectrum  $P$  by projection onto the subspace spanned by the orthonormal functions, i.e., by computing the respective scalar products

$$\bar{S}_i = \int_A \bar{P}(k_x, k_y) \bar{h}_i(k_x, k_y) dk_x dk_y, \quad 1 \leq i \leq n_\varphi n_k, \quad (25)$$

where  $\bar{P}$  is the normalized image spectrum

$$\bar{P} = P \cdot \left( \int_A P(k_x, k_y) dk_x dk_y \right)^{-1}. \quad (26)$$

By this normalization, the parameters  $\bar{S}_1, \dots, \bar{S}_{n_\varphi n_k}$  provide information on the shape of the SAR spectrum. This is particularly important for the estimation of the mean wave period, which is a normalized quantity by definition as well. It turned out that the normalization is also beneficial for the estimation of wave heights, which indicates that the shape of the SAR image spectrum contains information about integral ocean wave parameters as also suggested by the standard theory [Alpers et al., 1981; Hasselmann and Hasselmann, 1991].

[32] The periodogram of the wave mode imagette computed using an FFT algorithm is used as an estimate of  $P$ . No filtering as usually done in spectral estimation procedures is performed to keep the algorithm as simple as possible. The estimation errors are not regarded as critical

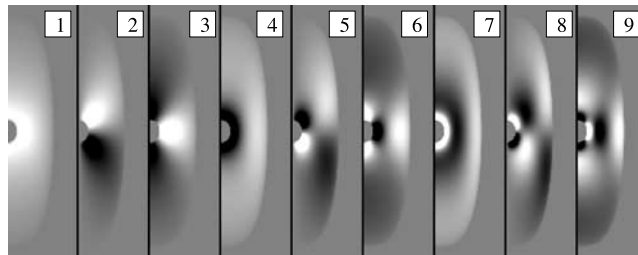


**Figure 5.** Orthonormal functions  $\bar{h}_1, \dots, \bar{h}_9$  defined in the spectral regime  $A$  (compare Figure 4) used to extract ocean wave information from the SAR image spectrum for  $n_\varphi = 3$  and  $n_k = 3$ . The grey values have a linear scaling between  $-80$  m (black) and  $+80$  m (white). Values below  $-80$  m or above  $+80$  m appear in black or white, respectively.

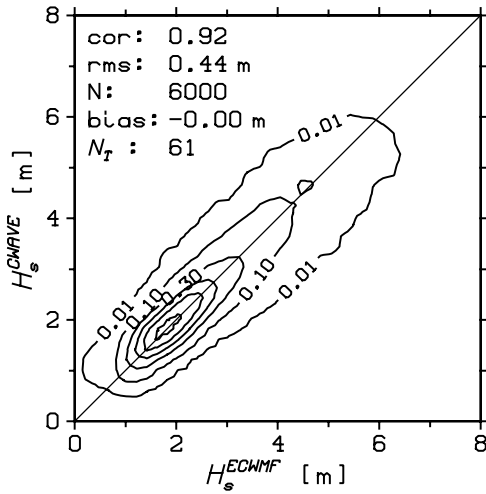


**Figure 6.** Scatter plot of significant wave heights estimated with the quadratic model equation (11) with 22 SAR parameters versus ECMWF wave heights based on a data set of 6000 collocation pairs.

for the algorithm because the SAR parameters are based on averages of larger spectral regimes (compare equation (25)).

[33] Using the two SAR parameters introduced in section 4 together with the new spectral parameters the vector  $\mathbf{s}$  defined in equation (5) is given by

$$\mathbf{s} = (\sigma_0, \text{cvar}, \bar{S}_1, \dots, \bar{S}_{n_{\phi n_k}}). \quad (27)$$

For the following calculations we have used  $n_{\phi} = 5$  and  $n_k = 4$ , i.e., the vector  $\mathbf{s}$  has 22 elements and the respective vector  $\mathbf{S}$  defined in equation (9) has the dimension  $n_f = 276$ .

[34] An important property of the CWAVE2.0 model is that the used SAR parameters have a hierarchical structure. The normalized variance *cvar* is scaling invariant with respect to the NRCS and the spectral parameters are scaling invariant with respect to both the NRCS and *cvar*. The parameters thus represent complementary information.

### 5.1. Significant Height

[35] The quadratic model with 22 parameters was tuned for the estimation of the significant wave height  $H_s$  by minimization of the cost function equation (10) using the data set described in section 2. The forward selection procedure described in section 3 terminated after  $N_T = 61$  iteration steps. The four dominating terms (neglecting the constant term) as selected by the method are as follows:

$$\bar{S}_3^2, \sigma_0, \text{cvar} \bar{S}_1, \sigma_0^2, \dots \quad (28)$$

[36] It is interesting to note that the dominating term contains pure spectral shape information. The subsequent terms contain information on both radar backscatter and image variance. The orthonormal function  $\bar{h}_3$  associated with the leading term can be found in Figure 5. As can be seen, the function extracts information on the energy differences between azimuthal and range travelling waves. This

observation could have to do with the azimuthal cutoff effect, but some further investigations are necessary to confirm this.

[37] The respective scatter plot generated from the test data set is shown in Figure 6. One can see a good correlation of above 0.9 with an rms of less than 0.5 m and a negligible bias. For the two examples in Figure 1 the CWAVE approach gave 8.1 m (Figure 1a) and 2.9 m (Figure 1b). The respective ECMWF analysis forecast was 8.1 m (Figure 1a) and 3.8 m (Figure 1b). It is interesting to note that the extended model leads to a significantly better agreement with the ECMWF data for the strong wind sea case compared to the two-parameter model described in section 4.

[38] A global map with the maximum CWAVE2.0 derived significant wave heights is shown in Figure 9c. The maximum was computed on 3 by 3 degree boxes using both the test and the training data set described in section 2. One can see several storm areas in particular on the Southern Hemisphere. Furthermore some higher waves can be found in the northern Atlantic, which are associated with Hurricane Fran, which hit the coast of Florida in early September 1996. The relative difference between the CWAVE2.0 derived wave height and the corresponding ECMWF wave heights is shown in Figure 9d. The colors correspond to the relative differences averaged over 3 by 3 degree boxes again for both the test and the tuning data set. It can be seen that the overall agreement is good. There is no clear correlation between the relative errors and either wind speed or wave heights (compare Figures 9b and 9c).

### 5.2. Spectral Bands

[39] In this section the energy contained in different spectral bands of the ocean wave spectrum is estimated with the CWAVE2.0 approach. This exercise has two objectives. First of all, parameters like  $H_{12}$  are actually used in practise and new approaches to estimate such parameters are desirable. Second, the application of the CWAVE approach on different spectral regimes can give insight into the performance and limitations of the method.

[40] For this purpose we define the wave height  $H_{T_1, T_2}$  corresponding to the spectral band defined by the limiting wave periods  $T_1$  and  $T_2$  as

$$H_{T_1, T_2} = 4 \left( \int_0^{2\pi} \int_{1/T_2}^{1/T_1} F_{\phi, f} df d\phi \right)^{1/2}. \quad (29)$$

[41] The tuning procedure was carried out for the wave heights  $H_{7,10}$ ,  $H_{10,13}$ ,  $H_{13,16}$ ,  $H_{16,19}$ , and  $H_{12}$ . The resulting scatterplots for the first four parameters are shown in Figures 7a–7d. The corresponding statistical parameters are summarized in Table 1. The table includes the respective parameters for the wave height  $H_{12} = H_{12, f_{min}-1}$  in addition. The third column of the table contains the corresponding range of wavelength assuming deep water. The overall good correlation shows that the empirical technique in fact provides useful information for both the longer swell dominated spectral regime as well as the wind sea part. The best correlation is observed for wavelength between 225 m and 400 m. It is interesting to note that the correlation is slightly worse for the longest considered waves between 400 m and 564 m wavelength although these waves should

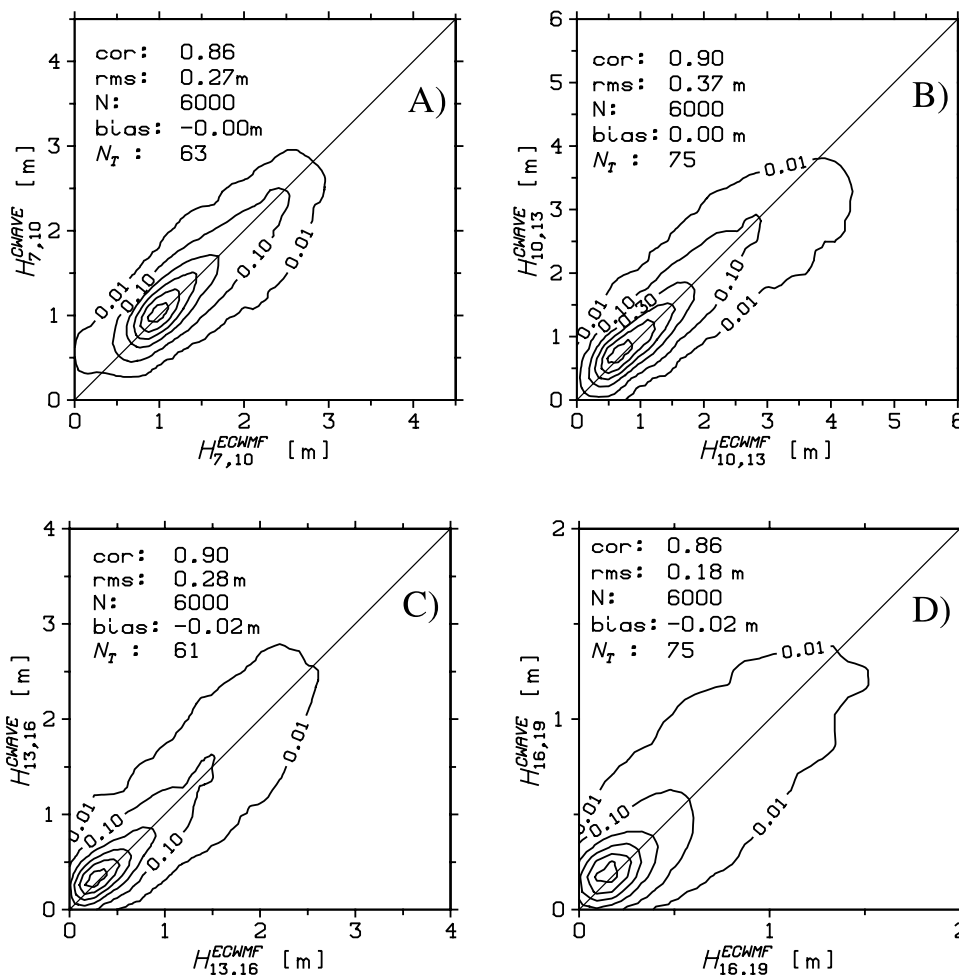


**Figure 7.** Scatter plots of CWAVE2.0 derived wave heights associated with different spectral bands according to the definition equation (29) with (a)  $H_{7,10}$ , (b)  $H_{10,13}$ , (c)  $H_{13,16}$ , and (d)  $H_{16,19}$  versus respective ECMWF wave heights.

be very well captured by the SAR according to the standard theory. This observation maybe explained by the performance of the WAM model version used in 1996 [Bidlot *et al.*, 2005], but some further studies making use of additional in situ data are necessary to clarify this point.

[42] A global map with the maximum wave heights  $H_{16,19}$  found on a 3 by 3 grid is shown in Figure 9e. Several areas with higher energy in the long wave regime can be observed in the South Pacific, South Atlantic, and South Indian Ocean. In most cases these waves are in the vicinity of strong storm events (compare Figure 9b), which generated long swell.

[43] For the examples in Figure 1 the CWAVE2.0 method results in 3.06 m (Figure 1a) and 1.54 m (Figure 1b) for  $H_{16,19}$ . The respective ECMWF wave heights are 3.31 m (Figure 1a) and 2.28 m (Figure 1b). The example shown in Figure 1b corresponds to the area of higher swell energy observed near the central west African coast.

### 5.3. Estimation of Mean Wave Periods

[44] Information on mean ocean wave periods is important for many applications. Although some attempts have been made to estimate mean periods from altimeter data [Caires *et al.*, 2005] the only spaceborne instrument, which provides direct spectral information on ocean waves, is still

the SAR sensor. There are various definitions of the mean wave period. The most elementary definition is

$$T_{m01} = \frac{m0}{m1}, \quad (30)$$

where the moments  $m_k$  are given by

$$m_k = \int f^k F_{f,\varphi} d\varphi df \quad k = 1, 2, \dots \quad (31)$$

**Table 1.** Statistical Parameters Describing the Performance of the CWAVE2.0 Approach in the Estimation of Wave Heights Corresponding to Different Spectral Bands<sup>a</sup>

Parameter	Periods, s	Wavelengths, m	Bias, m	rms, m	Cor	Mean, m
$H_{7,10}$	7–10	56–126	−0.004	0.27	0.84	1.31
$H_{10,13}$	10–13	126–264	0.01	0.37	0.87	1.33
$H_{13,16}$	13–16	264–400	0.02	0.33	0.90	0.78
$H_{16,19}$	16–19	400–564	−0.02	0.18	0.86	0.36
$H_{12}$	12–24	225–900	0.03	0.40	0.91	1.15
$H_s$	2.4–24	9.8–900	−0.004	0.45	0.92	2.55

<sup>a</sup>The values are based on a comparison with 6000 ECMWF model spectra. The mean refers to the CWAVE2.0 derived wave heights.

**Table 2.** Statistical Parameters Describing the Performance of the CWAVE Algorithm in the Estimation of Different Mean Ocean Wave Periods<sup>a</sup>

Mean Period	Cor	Bias, s	rms, s
$T_{m01}$	0.84	0.04	0.77
$T_{m02}$	0.78	0.02	0.80
$T_{m-10}$	0.84	0.05	0.80

<sup>a</sup>The parameters were computed based on a separate test data set of 6000 ERS-2 wave mode data and colocated ECMWF spectra.

More often used in practise is the zero upcrossing period, defined as

$$T_{m02} = \sqrt{\frac{m_0}{m_2}}. \quad (32)$$

Finally, there is the “energy wave period” given by

$$T_{m-10} = \frac{m_{-1}}{m_0}, \quad (33)$$

which is of relevance in the ocean energy sector [World Meteorological Organization (WMO), 1998] as explained in the next section.

[45] Using the same approach already used for the wave heights in section 5.1, the CWAVE2.0 model with 22 parameters was fitted for the estimation of the three different wave periods. The results obtained by applying the tuned model on the test data set are summarized in Table 2. One can see that the lowest correlation of 0.78 is found for  $T_{m02}$ . This is not surprising because this parameters has the strongest dependence on the high-frequency tail of the spectrum, which is particularly hard to access with the SAR sensor.

[46] A comparison of the CWAVE2.0 derived mean frequency  $T_{m-10}$  with ECMWF data is shown in Figure 8a. One can see a reasonable correlation of 0.86 with an rms of 0.72 s. As expected, there is a high-frequency cutoff period of about 6 s visible, which is due the resolution limit of the SAR system. In deep water waves with less than 6 s period have wavelength shorter than 60 m and cannot be seen by the ERS-2 SAR system.

[47] A global map with the mean Energy wave period  $T_{m-10}$  derived with CWAVE2.0 is shown in Figure 9f. We can see longer wave periods associated with strong storm

events, which generate long wind sea and swell waves, in particular on the southern hemisphere.

[48] For the examples shown in Figure 1 the approach gave 10.11 s (Figure 1a) and 9.98 s (Figure 1b) for the zero upcrossing period. The respective ECMWF periods are 10.02 s (Figure 1a) and 10.53 s (Figure 1b). Note that the two examples show almost the same mean period although the sea state characteristics is completely different.

#### 5.4. Estimation of Wave Power

[49] A key parameter for the exploitation of ocean wave energy is the wave power  $J$  defined as [WMO, 1998]

$$J = \alpha_P H_s^2 T_{m-10} \quad (34)$$

with a constant  $\alpha_P = 0.49 \text{ kW m}^{-3} \text{ s}^{-1}$ . Information on this quantity, which corresponds to the wave power per meter crest length, is for example needed for the optimal siting of ocean wave energy converters.

[50] Using 22 SAR parameters as input the quadratic model equation (11) was tuned for the estimation of  $J$ . The resulting scatter plot generated from the test data set described in section 2 is shown in Figure 8b. One can see a good correlation of 0.9 and a reasonable rms of 17.76 kW/m. For the examples in Figure 1 the CWAVE2.0 method results in 391.3 kW/m (Figure 1a) and 63.3 Kw/m (Figure 1b). The respective ECMWF wave powers are 406.9 kW/m (Figure 1a) and 98.9 kW/m (Figure 1b), respectively. Note that in the present setup the model is tuned with a large variety of sea states including the extreme wave conditions far offshore. To use this method for applications like the optimal siting of wave energy converters, the method should be retuned with a dedicated data set representing coastal wave conditions.

## 6. Buoy Comparisons

[51] In this section, CWAVE2.0 derived significant wave heights are compared to buoy measurements. The entire ERS-2 wave mode data set (including the tuning period) described in section 2.1 and 8000 additional imagettes acquired 4–9 October 1996 and 1 June 1997 were colocated with buoy data provided by the NDBC. The CWAVE2.0 model tuned as described in section 5.1 was used for this comparison.

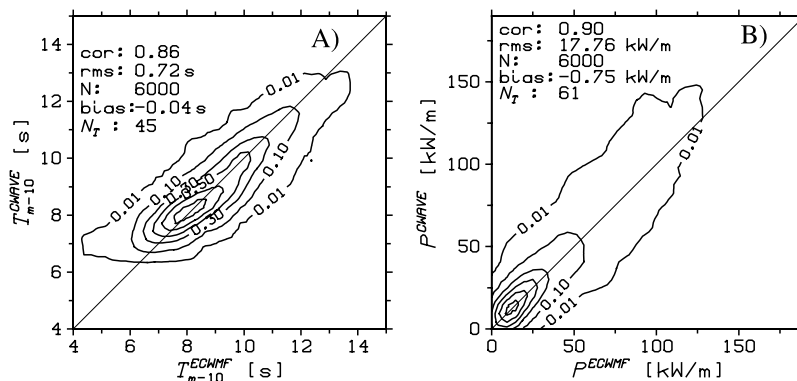


**Figure 8.** (a) Scatter plot of the mean period  $T_{m-10}$  derived from ERS-2 wave mode data compared to respective ECMWF model data. (b) The same as Figure 8a for the ocean wave power  $J$ .

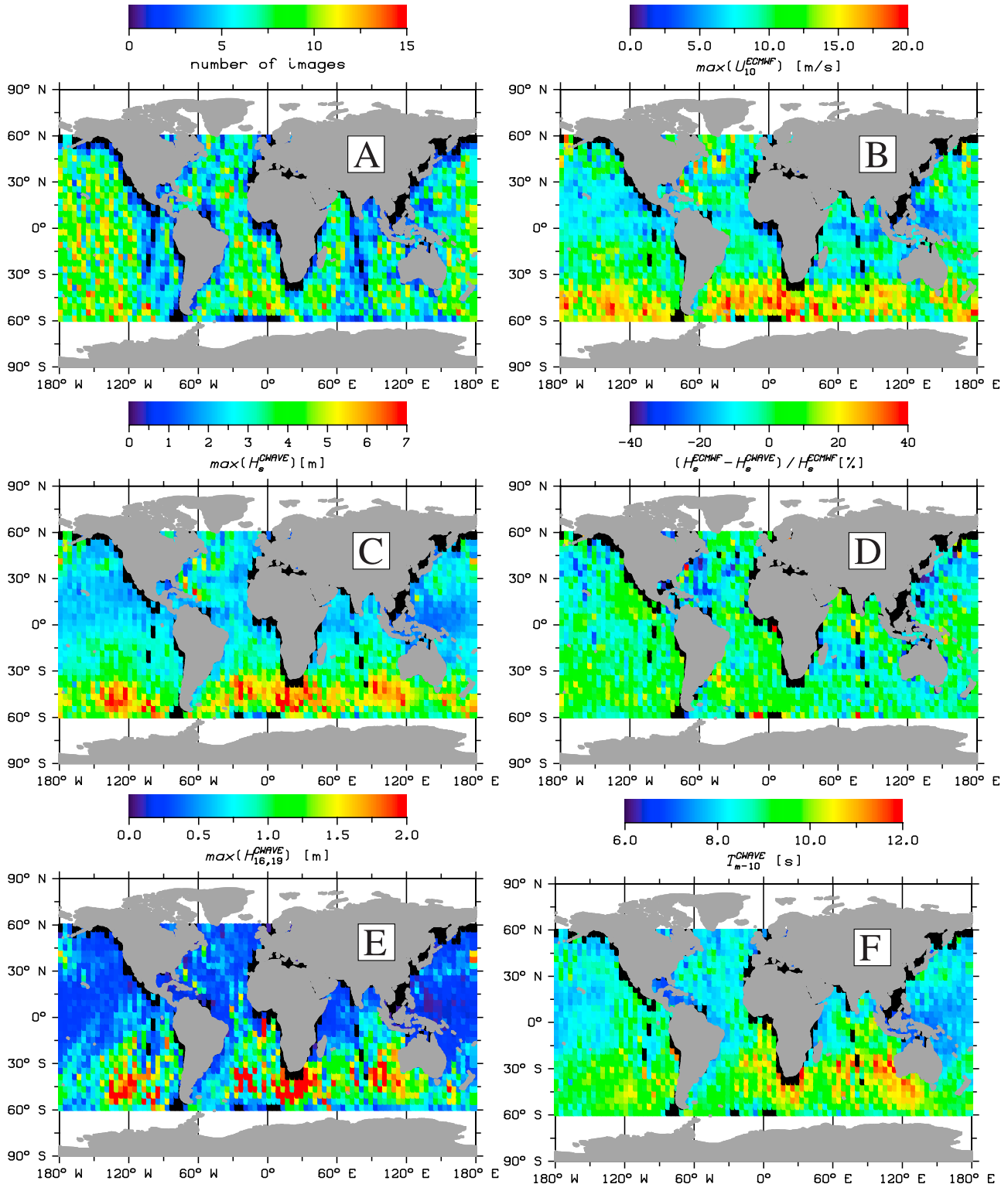


**Figure 9.** Global maps showing different parameters which refer to 3 by 3 degree boxes. The plots are based on 12,000 imagettes (tuning and test data together) taken between 23 August and 8 September 1996. (a) Number of imagettes. (b) Maximum ECMWF wind speeds. (c) Maximum CWAVE2.0 derived significant wave heights. (d) Averaged relative deviation between CWAVE2.0 and ECMWF wave heights. (e) Maximum of wave height  $H_{16,19}$  (compare equation (29)). (f) Average of mean period  $T_{m-10}$ .

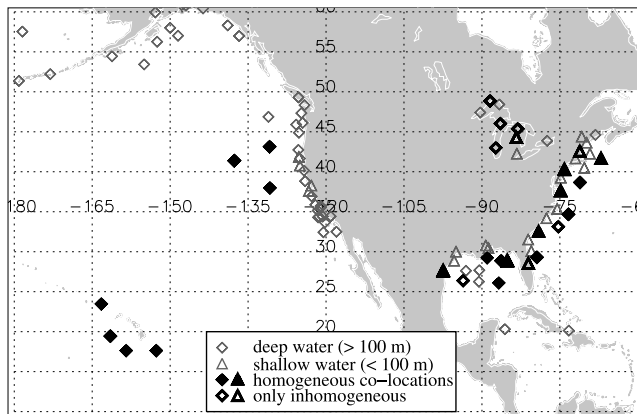


**Figure 10.** NDBC buoys used for comparisons with SAR retrieved wave heights. The diamonds indicate deep water (water depths  $>100$  m) and the triangles indicate shallow water. Thick black symbols represent buoys for which at least one collocation with ERS-2 wave mode data exists for the periods 23.8. –8.9.1996, 4.10.–9.10.1996, and 1.6.1997. The filled symbols indicate buoy locations where at least one homogeneous SAR image was found.

[52] The buoy data are freely available on the internet and consist of measurements of one-dimensional ocean wave spectra available every hour. The locations of the 97 buoys used for the collocation exercise are shown in Figure 10. Triangles represent buoys deployed at less than 100 m water depth. The remaining buoy locations in deeper water are indicated by diamonds. Only wave mode images with a distance less than 100 km from the buoys were taken into account. The thick black symbols in Figure 10 indicate buoys for which at least one collocated image was found. There are no collocations for the large number of buoys close to the U.S. west coast simply because no images were taken in that area at all during the analyzed period (compare Figure 9a).

[54] The collocation procedure resulted in 49 pairs of buoy measurements and SAR data. Applying the homogeneity test described in section 2.1 left 33 collocations for the comparison. The filled symbols in Figure 10 indicate buoys for which at least one homogeneous wave mode image was found. For example in the great lakes in the US all collocated images were found to be inhomogeneous.

[55] A scatter plot of buoy wave heights versus CWAVE2.0 estimations is shown in Figure 11. Diamonds refer to deep water buoys ( $>100$  m water depth) and triangles indicate the remaining shallow water measurements. The 12 shallow water cases are shown although a degradation of the algorithm performance is expected under such conditions as the tuning data set is dominated by deep water cases. For example the lower right outlier represents a shallow water case (88 m water depth) at the west coast of the Gulf of Mexico with 12.5 s dominant wave period according to the buoy measurement. The given statistical parameters refer to the 21 remaining deep water cases. One can see a good correlation of 0.95 and an rms around 0.4 m with a small bias of 6 cm. The dashed regression line indicates a slight underestimation of the SAR algorithm with respect to the buoy measurements for higher waves. A similar tendency of ECMWF analysis wave heights with

respect to buoy data is reported by *Janssen et al.* [1997] for the year 1995. It could therefore well be that the observed trend in the CWAVE2.0 derived wave heights is due to an analogue behavior of the tuning data set.

## 7. Conclusion

[57] A new empirical approach to estimate integral ocean wave parameters from SAR data has been presented. The method is called CWAVE2.0 and has the radiometrically calibrated SAR image as the only input. The approach is computationally efficient and of particular interest for users without easy access to numerical model data.

[58] The technique is based on a least squares approach with a quadratic model function as the core element. The model function was fitted using a global data set of 6000 ERS-2 wave mode data and collocated ECMWF wave model spectra. The performance of the retrieval technique was demonstrated on a separate data set of 6000 collocation pairs. Comparisons with ECMWF data were presented as tables of statistical parameters, scatterplots, and global maps.

[59] It was shown that a reasonable estimate of the significant wave height with an rms of about 0.6 m and a correlation of 0.86 can already be achieved based on a simple two-parameter model using the normalized radar cross section and the normalized image variance as the only input. An extended approach with 22 input parameters was presented, which makes use of additional spectral information leading to an even better rms of below 0.5 m and a correlation of above 0.9 for significant wave height.

[60] Significant wave heights estimated with the extended approach were also compared to NDBC buoy measurements. For deep water cases a correlation above 0.9 and an rms below 0.5 m was found. A slight tendency of the CWAVE2.0 algorithm to underpredict wave heights compared to the NDBC buoys at higher sea states could be

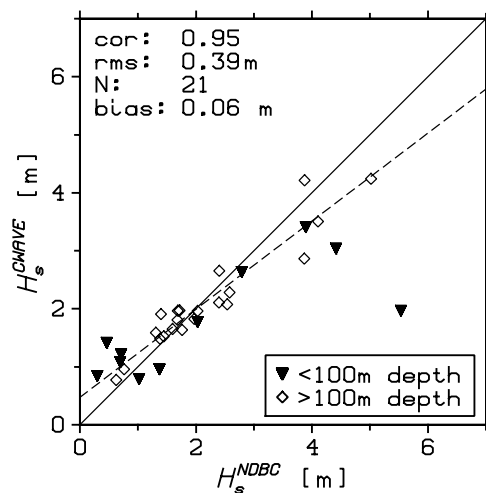


**Figure 11.** Comparison of significant wave height  $H_s$  derived from ERS-2 wave mode data with collocated NDBC buoy measurements. Triangles indicate deep water ( $>100$  m) and diamonds represent shallow water buoys. The statistical parameters and the dashed regression line refer to the deep water cases only.

explained by a similar tendency reported for the ECMWF tuning data set.

[61] The extended approach was then applied for the estimation of the three mean wave periods  $T_{m01}$ ,  $T_{m02}$ ,  $T_{m-10}$ . It was shown that with the CWAVE2.0 method SAR is able to provide useful information on these parameters, which are hardly measurable with other spaceborne instruments. The resulting rms is about 0.8 s in all three cases with correlations between 0.78 and 0.84. All three parameters show a high-frequency cutoff period of about 6 s, which is due to resolution limitations of the SAR system.

[62] Concerning the wave heights associated with different spectral bands, correlations of about 0.9 could be found for  $H_{12}$  and  $H_{13,16}$ . The lowest correlation of 0.84 was observed for the wave height  $H_{7,10}$  related to shorter waves. This again can be explained by the finite system resolution.

[63] Finally, the CWAVE2.0 approach was applied for the estimation of the wave power  $J$ , which is a function of both significant wave height and the mean period  $T_{m-10}$ . Comparisons with ECMWF data showed a promising correlation of 0.9 with an rms of 17.8 kW/m. We expect that the proposed new technique will be a driver for the use of SAR data, e.g., for the optimal siting of wave energy converters.

[64] The implications of the choice of tuning data were discussed. For example in the context of wave power it is obvious that the model should be retuned using a dedicated data set, which represents typical wave conditions at the coast, rather than average sea states on a global scale.

[65] It was also emphasized that the cost function formulation used in this study is based on rather simplifying assumptions. A more sophisticated formulation is possible using weighting functions, which add information on the error statistics of the tuning data set. With the help of weighting functions it is also possible to focus on special wave conditions, e.g., in order to improve wave height estimates in extreme sea states.

[66] Further work is also necessary to link the empirical model to existing theoretical descriptions of the SAR imaging process. On the one hand, the achieved results may help to fine tune uncertain parameters in the physical models; on the other hand, certain elements of the theoretical formulation could be integrated into the empirical approach to further improve the performance.

[67] The techniques described in this study are currently applied to a larger data set of two years of ERS-2 wave mode data, which are reprocessed at DLR from raw data provided by ESA in the framework of the ERS AO WaveAtlas. In order to better understand the impact of the tuning data set additional comparisons with buoy data are on the way.

## Appendix A: Least Squares Minimization

[68] The estimation of the fit parameter vector  $\mathbf{A}$  as given by equation (10) is a standard linear least squares minimization problem, which was solved using a singular value decomposition technique [Press *et al.*, 1992]. Let us define the design matrix  $C$  by

$$C = \begin{pmatrix} 1 & S_1^{(1)} & \dots & S_{n_f-1}^{(1)} \\ \vdots & \vdots & \vdots & \vdots \\ 1 & S_1^{(N)} & \dots & S_{n_f-1}^{(N)} \end{pmatrix}. \quad (\text{A1})$$

The minimization problem can then be written as

$$\text{minimise } J_{\text{cost}}(\mathbf{A}) = \|\mathbf{C}\mathbf{A} - \mathbf{w}\|^2, \quad (\text{A2})$$

where  $\mathbf{w} = (w^{(1)}, \dots, w^{(N)})$  is the vector of measurements. Applying a singular value decomposition to the matrix  $C$  yields

$$C = U D V^T \quad (\text{A3})$$

with a diagonal matrix  $D = \text{diag}(s_1, \dots, s_{n_f})$  containing the singular values and two orthogonal matrices  $U$  and  $V$ . The solution of the least squares problem can then be written as

$$\mathbf{A} = \sum_{i=1}^{n_f} \left( \frac{\mathbf{U}_{(i)} \cdot \mathbf{w}}{s_i} \right) \mathbf{V}_{(i)}, \quad (\text{A4})$$

where the columns of  $V$  and  $U$  are denoted by  $\mathbf{V}_{(1)}, \dots, \mathbf{V}_{(n_f)}$  and  $\mathbf{U}_{(1)}, \dots, \mathbf{U}_{(n_f)}$ , respectively.

## Appendix B: Orthonormal Functions

[69] In the following the construction of the orthonormal functions used in section 5 is explained. In principle such a set of functions could also be derived empirically using an EOF analysis; however, the objective here was to keep the method in an analytical form as far as possible to allow an easy reproduction of the results.

[70] The exact definition of the area  $A$  (compare Figure 4) is given by the transformation

$$\alpha_k(k_x, k_y) = 2 \frac{\log \sqrt{a_1 k_x^4 + a_2 k_x^2 + k_y^2} - \log k_{\min}}{\log k_{\max} - \log k_{\min}} - 1 \quad (\text{B1})$$

$$\alpha_\varphi(k_x, k_y) = \arctan(k_y, k_x),$$

which maps  $A$  onto the rectangle  $B = [-1, 1] \times [-\pi/2, \pi/2]$ . The parameters  $a_1, a_2$  are defined as

$$a_1 = \frac{\gamma^2 - \gamma^4}{\gamma^2 k_{\min}^2 - k_{\max}^2} \quad (\text{B2})$$

$$a_2 = \frac{k_{\max}^2 - \gamma^4 k_{\min}^2}{k_{\max}^2 - \gamma^2 k_{\min}^2}. \quad (\text{B3})$$

[71] The following values for  $k_{\max}$ ,  $k_{\min}$  and the bunching parameter  $\gamma$  were used in this study:

$$\gamma = 2 \quad (\text{B4})$$

$$k_{\max} = 2\pi (60 \text{ m})^{-1} \quad (\text{B5})$$

$$k_{\min} = 2\pi (624 \text{ m})^{-1} \quad (\text{B6})$$

The bunching parameter  $\gamma$  gives the ratio of the highest range and azimuth wave numbers found in the domain  $A$ . Note that  $\gamma$  does not affect the longer waves, i.e., the inner boundary of the area  $A$  has a circular shape. The value for  $k_{\min}$  corresponds to waves of 20 s period assuming deep water [Phillips, 1977]. We excluded the longest waves above 624 m up to 895 m contained in the WAM model (compare section 2) to avoid contamination by atmospheric structures like, e.g., boundary layer rolls [Alpers and Brümmer, 1994]. The minimum wavelength considered is in the order of twice the system resolution in the range direction.

[72] The orthonormal functions are composed of Gegenbauer polynomial  $C_n^\lambda$  with  $\lambda = 3/2$  [Gradshteyn and Ryzhik, 2000] and harmonic functions. The use of these polynomials is motivated by the fact that the respective projections are weighted by a function which is zero at the lower and upper wave number boundaries of the regime  $A$ . This makes sense because the spectral energy in these regimes is usually very small [Lehner et al., 2000]. Hence for the wave number dimension of the spectrum the set of functions

$$\begin{aligned} g_1(\alpha_k) &= \frac{1}{2} \sqrt{3} \nu(\alpha_k) \\ g_2(\alpha_k) &= \frac{1}{2} \sqrt{15} \alpha_k \nu(\alpha_k) \end{aligned} \quad (B7)$$

$$\begin{aligned} g_3(\alpha_k) &= \frac{1}{4} \sqrt{\frac{7}{6}} (15 \alpha_k^2 - 3) \nu(\alpha_k) \\ \vdots &= \vdots \end{aligned} \quad (B8)$$

$$g_{n_k}(\alpha_k) = \sqrt{\frac{n_k + 3/2}{(n_k + 2)(n_k + 1)}} C_{n_k}^{3/2} \nu(\alpha_k) \quad (B9)$$

is used with  $\nu$  defined as

$$\nu(\alpha_k) = \sqrt{1 - \alpha_k^2}. \quad (B10)$$

The functions  $g_1, \dots, g_{n_k}$  are orthonormal on the interval  $[-1, 1]$ .

[73] The angular dimension is described using the  $\pi$ -periodic harmonics

$$\begin{aligned} f_1(\alpha_\varphi) &= \sqrt{\frac{1}{\pi}} \\ f_2(\alpha_\varphi) &= \sqrt{\frac{2}{\pi}} \sin(2 \alpha_\varphi) \\ f_3(\alpha_\varphi) &= \sqrt{\frac{2}{\pi}} \cos(2 \alpha_\varphi) \\ \vdots &= \vdots \\ f_{n_\varphi-1}(\alpha_\varphi) &= \sqrt{\frac{2}{\pi}} \sin((n_\varphi - 1) \alpha_\varphi) \\ f_{n_\varphi}(\alpha_\varphi) &= \sqrt{\frac{2}{\pi}} \cos((n_\varphi - 1) \alpha_\varphi), \end{aligned} \quad (B11)$$

where  $n_\varphi$  is an odd number. The functions

$$h_{ij}(\alpha_k, \alpha_\varphi) = g_i(\alpha_k) f_j(\alpha_\varphi) \quad 1 \leq i \leq n_k \quad 1 \leq j \leq n_\varphi \quad (B12)$$

then represent an orthonormal system on the rectangle  $B$ . Hence the functions

$$\begin{aligned} \bar{h}_{n_\varphi(i-1)+j}(k_x, k_y) &= \eta(k_x, k_y) g_i(\alpha_k(k_x, k_y)) f_j(\alpha_\varphi(k_x, k_y)) \\ & \quad 1 \leq i \leq n_k \quad 1 \leq j \leq n_\varphi \end{aligned} \quad (B13)$$

are orthonormal on the elliptic area  $A$  with a function  $\eta$  defined as

$$\eta(k_x, k_y) = \left( \frac{2(a_2 k_x^2 + 2a_1 k_x^4 + k_y^2)}{(k_x^2 + k_y^2)(a_2 k_x^2 + a_1 k_x^4 + k_y^2)(\log k_{\max} - \log k_{\min})} \right)^{1/2}. \quad (B14)$$

[74] **Acknowledgments.** We would like to thank the European Space Agency (ESA) for providing ERS-2 wave mode raw data in the framework of the ERS-AO3 project COMPLEX (ID 999192) and WAVEATLAS (ID 2342). Part of this work was carried out in the framework of the Virtual Institute EXTROP as well as the Research Network IEOS funded by the Helmholtz Association of German Research Centers (HGF). We thank ECMWF for technical advice concerning WAM model data. We are grateful for free access to buoy measurements provided by NOAA's National Data Buoy Center (NDBC). Finally, we thank the reviewers for their careful reading of the manuscript and a lot of constructive hints and comments.

## References

- Abdalla, S., J.-R. Bidlot, and P. Janssen (2006), Global validation and assimilation of ENVISAT ASAR wave mode spectra, paper presented at 2006 SEASAR Workshop, Eur. Space Agency, Frascati, Italy.
- Alpers, W., and B. Brümmer (1994), Atmospheric boundary layer rolls observed by the synthetic aperture radar aboard the ERS-1 satellite, *J. Geophys. Res.*, *99*, 12,613–12,621.
- Alpers, W. R., D. B. Ross, and C. L. Rufenach (1981), On the detectability of ocean surface waves by real and synthetic aperture radar, *J. Geophys. Res.*, *86*, 6481–6498.
- Attema, E. (2005), Mission requirements document for the European radar observatory Sentinel-1, Rep. ES-RS-ESA-SY-0007, Eur. Space Agency, Noordwijk, Netherlands.
- Bidlot, J.-R., D. Holmes, P. Wittemann, R. Lalbeharry, and H. Chen (2002), Intercomparison of the performance of operational wave forecasting systems with buoy data, *Weather Forecasting*, *17*, 287–310.
- Bidlot, J.-R., P. Janssen, and S. Abdalla (2005), On the importance of spectral wave observations in the continued development of global wave models, paper presented at WAVES 2005: Fifth International Symposium on Ocean Wave Measurements and Analysis, Centro de Estud. y Exp. de Obras Públicas, Madrid, Spain.
- Caires, S., A. Sterl, and C. Gommenginger (2005), Global ocean mean wave period data: validation and description, *J. Geophys. Res.*, *110*, C02003, doi:10.1029/2004JC002631.
- Gradshteyn, L., and L. Ryzhik (2000), *Table of Integrals, Series, and Products*, Elsevier, New York.
- Hasselmann, K., and S. Hasselmann (1991), On the nonlinear mapping of an ocean wave spectrum into a synthetic aperture radar image spectrum, *J. Geophys. Res.*, *96*, 10,713–10,729.
- Hasselmann, S., C. Brüning, K. Hasselmann, and P. Heimbach (1996), An improved algorithm for the retrieval of ocean wave spectra from synthetic aperture radar image spectra, *J. Geophys. Res.*, *101*, 16,615–16,629.
- Horstmann, J., H. Schiller, J. Schulz-Stellenfleth, and S. Lehner (2003), Global wind speed retrieval from SAR, *IEEE Trans. Geosci. Remote Sens.*, *41*, 2277–2286.
- Janssen, P. (2004), *The Interaction of Ocean Waves and Wind*, 300 pp., Cambridge Univ. Press, New York.
- Janssen, P., B. Hansen, and J.-R. Bidlot (1997), Verification of the ECMWF wave forecasting system against buoy and altimeter data, *Weather Forecasting*, *12*, 763–784.
- Janssen, P., J.-R. Bidlot, S. Abdalla, and H. Hersbach (2005), Progress in ocean wave forecasting at ECMWF, Tech. Memo 478, Eur. Cent. for Medium-Range Weather Forecasts, Reading, UK.
- Johnsen, H., G. Engen, B. Chapron, N. Walker, and Y.-L. Desnos (2002), The ASAR Wave Mode: Level 1 and 2 Algorithms and Products, paper presented at ENVISAT Calibration Review, 9-13 September 2002, Eur. Space Agency, Noordwijk, Netherlands.

- Kerbaol, V. (1997), Analyse spectrale et statistique vent-vagues des images radar a ouverture synthetique, Ph.D. thesis, Univ. de Rennes, Rennes, France.
- Kerbaol, V., B. Chapron, and P. W. Vachon (1998), Analysis of ERS-1/2 synthetic aperture radar wave mode images, *J. Geophys. Res.*, *103*, 7833–7846.
- Laur, H., P. Bally, P. Meadows, J. Sanchez, B. Schaettler, and E. Lopinto (1996), Derivation of the backscattering coefficient  $\sigma_0$  in ESA ERS-1/2 SAR PRI data products, technical report, Eur. Space Agency, Noordwijk, Netherlands.
- Lehner, S., J. Horstmann, W. Koch, and W. Rosenthal (1998), Mesoscale wind measurements using recalibrated ERS SAR images, *J. Geophys. Res.*, *103*, 7847–7856.
- Lehner, S., J. Schulz-Stellenfleth, B. Schättler, H. Breit, and J. Horstmann (2000), Wind and wave measurements using complex ERS-2 SAR wave mode data, *IEEE Trans. Geosci. Remote Sens.*, *38*, 2246–2257.
- Mastenbroek, C., and C. F. de Valk (2000), A semi-parametric algorithm to retrieve ocean wave spectra from synthetic aperture radar, *J. Geophys. Res.*, *105*, 3497–3516.
- Phillips, O. M. (1977), *Dynamics of the Upper Ocean*, Cambridge Univ. Press, New York.
- Press, W. H., S. A. Teukolsky, W. T. Vetterling, and B. P. Flannery (1992), *Numerical Recipes in FORTRAN: The Art of Scientific Computing*, Cambridge Univ. Press, New York.
- Schulz-Stellenfleth, J., and S. Lehner (2004), Measurement of 2-d sea surface elevation fields using complex synthetic aperture radar data, *IEEE Trans. Geosci. Remote Sens.*, *42*, 1149–1160.
- Schulz-Stellenfleth, J., S. Lehner, and D. Hoja (2005a), A parametric scheme for the retrieval of 2-d ocean wave spectra from synthetic aperture radar look cross spectra, *J. Geophys. Res.*, *110*, C05004, doi:10.1029/2004JC002822.
- Schulz-Stellenfleth, J., J. Nieto-Borge, and A. Niedermeier (2005b), SAR ocean wave measurements based on empirical imaging model, paper presented at 2005 International Geoscience and Remote Sensing Symposium, IEEE, Seoul, South Korea.
- Stoffelen, A., and D. Anderson (1997), Scatterometer data interpretation: Estimation and validation of the transfer function CMOD4, *J. Geophys. Res.*, *102*, 5767–5780.
- von Storch, H., and F. Zwiers (1999), *Statistical Analysis in Climate Research*, Cambridge Univ. Press, New York.
- World Meteorological Organization (WMO) (1998), T, Rep. 702, 2nd ed., Geneva. (Available at <http://www.wmo.ch/index-en.html>.)
- 
- T. König, S. Lehner, and J. Schulz-Stellenfleth, Remote Sensing Technology Institute, German Aerospace Center (DLR), Oberpfaffenhofen, D-82234 Wessling, Germany. (johannes.schulz-stellenfleth@dlr.de)